EJN fens European Journal of Neuroscience

European Journal of Neuroscience, Vol. 35, pp. 1692–1704, 2012 doi:10.1111/j.1460-9568.2012.08078.x

MOLECULAR AND DEVELOPMENTAL NEUROSCIENCE

Computational molecular phenotyping of retinal sheet transplants to rats with retinal degeneration

M. J. Seiler,[1,2,*] B. W. Jones,[3,*] R. B. Aramant,[1] P. B. Yang,[1] H. S. Keirstead[1,2] and R. E. Marc[3]
[1]Anatomy & Neurobiol/Reeve-Irvine Research Center, UC Irvine, Irvine, CA 92697-4265, USA
[2]Sue & Bill Gross Stem Cell Research Center, UC Irvine, Irvine, CA, USA
[3]Ophthalmology, Moran Eye Center, University of Utah, Salt Lake City, UT, USA

Keywords: CRALBP, electron microscopy, GABA, molecular phenotyping, retinal transplantation, synaptic circuitry

Abstract

Retinal progenitor sheet transplants have been shown to extend neuronal processes into a degenerating host retina and to restore visual responses in the brain. The aim of this study was to identify cells involved in transplant signals to retinal degenerate hosts using computational molecular phenotyping (CMP). S334*ter* line 3 rats received fetal retinal sheet transplants at the age of 24–40 days. Donor tissues were incubated with slow-releasing microspheres containing brain-derived neurotrophic factor or glial cell-derived neurotrophic factor. Up to 265 days after surgery, eyes of selected rats were vibratome-sectioned through the transplant area (some slices stained for donor marker human placental alkaline phosphatase), dehydrated and embedded in Eponate, sectioned into serial ultrathin datasets and probed for rhodopsin, cone opsin, CRALBP (cellular retinaldehyde binding protein), L-glutamate, L-glutamine, glutathione, glycine, taurine, γ-aminobutyric acid (GABA) and DAPI (4′,6-diamidino-2-phenylindole). In large transplant areas, photoreceptor outer segments in contact with host retinal pigment epithelium revealed rod and cone opsin immunoreactivity whereas no such staining was found in the degenerate host retina. Transplant photoreceptor layers contained high taurine levels. Glutamate levels in the transplants were higher than in the host retina whereas GABA levels were similar. The transplant inner nuclear layer showed some loss of neurons, but amacrine cells and horizontal cells were not reduced. In many areas, glial hypertrophy between the host and transplant was absent and host and transplant neuropil appeared to intermingle. CMP data indicate that horizontal cells and both glycinergic and GABAergic amacrine cells are involved in a novel circuit between transplant and host, generating alternative signal pathways between transplant and degenerating host retina.

Introduction

Retinal degenerative diseases such as age-related macular degeneration or retinitis pigmentosa lead to progressive vision loss and, ultimately, total blindness in millions of people worldwide. When photoreceptor loss occurs, the neural retina beneath demonstrates plasticity, and continues to signal in the absence of photoreceptor input (Margolis *et al.*, 2008; Jensen & Rizzo, 2009; Kolomiets *et al.*, 2010), albeit with early reprogramming in glutamate receptor expression and alterations in retinal circuitry (Strettoi *et al.*, 2003; Marc *et al.*, 2007, 2008; Lin *et al.*, 2009). This prolonged function along with demonstrated plasticity in the remnant neural degenerate retina may define windows of opportunity for intervention (Jones *et al.*, 2003) and raises the possibility of therapies based upon the replacement of diseased cells with retinal progenitors. Transplanted cells may be able to integrate into the remodeling retina and form functional connections with the host retina, ultimately assisting with retinal repair and vision improvement.

Correspondence: Prof H. S. Keirstead, as above.
E-mail: hansk@uci.edu

*M.J.S. and B.W.J. contributed equally to this study.

Received 12 January 2012, revised 13 February 2012, accepted 15 February 2012

Methodologies have been developed to transplant freshly harvested sheets of fetal retinal progenitor cells with or without retinal pigment epithelium (RPE) to the subretinal space (Aramant & Seiler, 2004; Radtke *et al.*, 2008; Seiler *et al.*, 2008a), which preserve the three-dimensional topology, resembling a normal retina (reviewed by Aramant & Seiler, 2004). In contrast, with dissociated retinal progenitor cells, photoreceptors do not survive in long-term transplants (Mansergh *et al.*, 2010) although – in microaggregate transplants – photoreceptors can survive for 8 months (Gouras & Tanabe, 2003).

Retinal sheet transplants restore visual responses in retinal degenerative models in a retinotopic manner in the superior colliculus (SC) (Woch *et al.*, 2001; Sagdullaev *et al.*, 2003; Thomas *et al.*, 2004; Yang *et al.*, 2010). SC recording is an established method to demonstrate photoreceptor rescue by RPE transplants (Sauvé *et al.*, 1998). Synaptic connections between transplant and host are implied through trans-synaptic tracing from the visually responsive site in the SC back to the transplant with attenuated pseudorabies virus (Seiler *et al.*, 2008c), and established directly by demonstrating synapses of transplant neurons in the host inner plexiform layer (IPL) at the ultrastructural level with transplants that had restored visual responses in the SC (Seiler *et al.*, 2010).

The retinal degeneration model used in this study was the transgenic pigmented S334*ter* line 3 rat (Steinberg *et al.*, 1996) expressing a mutated truncated rhodopsin gene resulting in a protein lacking the 15 carboxyl-terminal amino acids involved in the rhodopsin transport to the outer segments (Lee & Flannery, 2007; Lin & LaVail, 2010). Similar mutations within the rhodopsin C terminus have been found in retinitis pigmentosa patients (Berson *et al.*, 2002) and lead to photoreceptor cell death (Liu *et al.*, 1999; Green *et al.*, 2000).

The goal of the current study was to investigate the potential circuitry of long-term retinal progenitor sheet transplants that had restored responses in the SC, using computational molecular phenotyping (CMP), a technique to transform anatomical data into multidimensional signatures, resulting in cell classification and quantitative visualization as tissue theme maps (Marc & Jones, 2002; Jones *et al.*, 2003).

Materials and methods

Ethics statement

For all experimental procedures, animals were treated in accordance with the NIH guidelines for the care and use of laboratory animals and the ARVO Statement for the Use of Animals in Ophthalmic and Vision Research, and under protocol 2006–2698 approved by the Institutional Animal Care and Use Committee of the University of California, Irvine (animal welfare assurance number A3416-01). All efforts were made to use only the minimum number of animals necessary to provide an adequate sample size.

Experimental animals

Donor rats with normal retina were bred from transgenic rats positive for human placental alkaline phosphatase (hPAP) (Kisseberth *et al.*, 1999; Mujtaba *et al.*, 2002); breeders were a gift of Dr Eric Sandgren (University of Wisconsin, Madison, WI, USA) and ACI rats were obtained from Harlan Laboratories (Indianapolis, IN, USA). RD rats were the F1 generation of a cross between albino homozygous S334*ter* line 3 and pigmented Copenhagen rats (Harlan Laboratories). This line was originally produced by Xenogen Biosciences (formerly Chrysalis DNX Transgenic Sciences, Princeton, NJ, USA), and was supplied with the support of the National Eye Institute by Dr Matthew LaVail, University of California, San Francisco (http://www.ucsfeye.net/mlavailRDratmodels.shtml).

Donor tissue

Fetal donor retina was dissected from fetuses of timed-pregnant hPAP donors that were determined to be hPAP-positive transgenic by a histochemical reaction for hPAP (Kisseberth *et al.*, 1999; Yang *et al.*, 2010). Fetuses and dissected retinas were stored in Hibernate E medium on ice or at 4 °C as previously described (Seiler *et al.*, 2008b, 2010). In some of the experiments, retinal flatmounts were incubated with brain-derived neurotrophic factor (BDNF) or glial cell-derived neurotrophic factor (GDNF) microspheres overnight (Seiler *et al.*, 2008b; Yang *et al.*, 2010). Before transplantation, retinas were cut into rectangular pieces of ca. 1 mm^2 to fit the flat nozzle of a custom-made implantation tool.

Transplantation

Thirteen transgenic S334*ter* line 3 RD rats expressing mutated human rhodopsin protein (Sagdullaev *et al.*, 2003; Ray *et al.*, 2010) were selected for this study (Table 1). Additional control rats for electrophysiology received transplants of fetal cortex or sham surgery. After ketamine/xylazine anesthesia (37.5 mg/kg ketamine, 5 mg/kg xylazine), rats received fetal retinal sheet transplants in one eye at postnatal day (P) 24–41 (10 different surgery days), as previously described (Seiler & Aramant, 1998; Aramant & Seiler, 2002). Briefly, after pupil dilation with 1% atropine (Bausch & Lomb, Tampa, FL, USA), and local anesthesia by tetracaine eye drops (0.5%) (Bausch & Lomb), the sclera was exposed, and a small cut (approximately 1.0 mm) was made parallel to the limbus and posterior to the pars plana. The implantation instrument was inserted into the subretinal space and advanced to the nasal quadrant close to the optic disk. Release of the instrument placed the tissue into the subretinal space, after which the instrument was withdrawn. The lesion was closed with 10-0 sutures and the eyes were treated with gentamycin and artificial tears ointment. Rats were placed in an incubator for recovery, and correct placement of the transplant into the subretinal space was confirmed by postsurgical fundus exams and ocular coherence tomography.

TABLE 1. Overview of experiments

Rat	Sex	Age at surgery (days)	Donor tissue	Survival time (days)	Age when killed (days)	Remarks
1	F	40	E19 retina	256	296	Laminated area (7 of 12 slices), no recording
2	M	41	E19 retina + BDNF	249	290	Laminated area (6 of 12 slices), no recording
3	F	35	E19 retina + BDNF	251	286	Laminated area (3 of 11 slices), no recording
4	F	24	E19 retina + GDNF	200	224	Mostly rosettes, laminated area in center of graft (4 of 9 slices), no recording
5	F	32	E19 retina + GDNF	87	129	Mostly rosettes, small laminated area (5 of 11 slices); SC recording, threshold −2.66 log cd/m^2
6	F	35	E19 retina + BDNF	251	286	Laminated area (7 of 11 slices), no recording
7	F	26	E19 retina + GDNF	130	155	Laminated area (9 of 13 slices); SC recording, threshold −2.2 log cd/m^2
8	F	32	E19 retina + GDNF	130	162	Laminated area (5 of 12 slices); SC recording, threshold −1.5 log cd/m^2
9	F	32	E19 retina + GDNF	77	110	Laminated areas (8 of 11 slices); SC recording, threshold −2.0 log cd/m^2
10	M	33	E19 retina	88	121	Mostly rosettes, small laminated area (3 of 10 slices); SC recording, threshold −2.5 log cd/m^2
11	F	37	E19 retina + BDNF	92	129	Mainly rosettes, tiny laminated area (5 of 12 slices); SC recording, threshold −2.2 log cd/m^2
12	F	25	E19 retina + GDNF	125	150	Rosettes only (7 slices); SC recording, threshold −0.9 log cd/m^2
13	M	33	E19 retina + GDNF	69	102	Rosettes only (11 slices); SC recording, threshold −1.5 log cd/m^2

SC recording

The visual responses to a full-field light stimulus were recorded in eight rats, 69–130 days after transplantation according to a previously described procedure (Thomas *et al.*, 2005; Yang *et al.*, 2010). Briefly, rats were dark-adapted overnight, anesthetized with ketamine/xylazine and placed into a stereotaxic apparatus under isoflurane anesthesia. All procedures were performed in the dark under dim red light. After a craniotomy, the surface of the SC was exposed. Using tungsten microelectrodes (0.5 MΩ impedance; MicroProbe Inc., Gaithersburg, MD, USA), multi-unit extracellular responses were recorded systematically from various sites of the SC (max. 0.3 mm depth) following a 40-ms light stimulus (luminance −5.0 to +1.0 log cd/m^2), using a digital data acquisition system (Powerlab; ADI Instruments, Mountain View, CA, USA). Stimuli were repeated at each site 10 times at 10-s intervals. A response was defined across the set of 10 photic stimuli as > 10% increase of spike counts over baseline or 10 spikes in the case of zero baseline activity. Visual responses were characterized for the location within the SC, response threshold, spike counts and response latencies. A one-way analysis of variance (ANOVA) with subsequent *post-hoc* tests from a statistics package of GraphPad Software Inc. (San Diego, CA, USA) was used for statistical comparisons (significance criterion $P < 0.05$).

Tissue processing

After anesthesia with an overdose of ketamine/xylazine, rats were perfused through the ascending aorta with 100 mL saline, followed by a 10-min perfusion of 300 mL fixative [1% paraformaldehyde, 2.5% glutaraldehyde, 3% sucrose (w/v), 1 mM $MgSO_4$ in 0.1 M sodium phosphate buffer, pH 7.4]. After enucleation and removal of the cornea, eyes were postfixed in the same fixative overnight, and washed three times with phosphate buffer. Eye cups were dissected to obtain cross-sections through the transplant area along the dorsoventral (superior–inferior) axis, embedded in 4% agarose and cut on a Leica VT 1000 S vibratome (Leica Instruments, Nussloch, Germany) at 70–100 μm. Some slices were stained for the donor label hPAP using BCIP/NBT (5-bromo-4-chloro-3-indolyl phosphate/nitro blue tetrazolium chloride; B-1911; Sigma, St. Louis, MO, USA) resulting in a blue–purple stain (Kisseberth *et al.*, 1999; Yang *et al.*, 2010). Selected vibratome slices were processed as previously described (Marc & Jones, 2002). Briefly, sections were dehydrated in a graded methanol series, followed by 100% acetone and infiltration with increasing concentrations of Eponate 812 (Ted Pella, Redding, CA, USA) in acetone. After infiltration with 100% eponate, the slices were flat-embedded, sandwiched between two Aclar films (Electron Microscopy Sciences, Hatfield, PA, USA) on glass slides, cured overnight at 65 °C, cut out and glued onto Epon stubs for ultrathin sectioning.

Electron microscopy

Semithin and ultrathin sections (70 nm thick) were cut from selected BCIP-stained blocks. Ultrathin sections were either left unstained or stained for 10 s with uranylacetate, and viewed in a JEOL1400 electron microscope at magnifications between 1500 and 15 000×.

Quantification of donor-specific hPAP label in thin sections of transplanted fetal retinas in S334ter rat retinas

Serial 200-nm thin sections were imaged at 8-bit 1388 pixel × 1036 line frames under voltage-regulated tungsten halogen flux with a variation of 1.2 ± 0.6%/min (mean ± SD). Image mosaic tiles were captured with a Peltier-cooled QImaging Fast 1394 QICAM (QImaging, Burnaby, BC, Canada) and a Syncroscan montaging system (Synoptics Inc., Frederick, MD, USA) on a Scan 100 × 100 stage (Märzhäuser, Wetzlar, Germany).

Every retina was imaged in a spectral series at 400, 450, 500, 550, 600 and 650 nm to verify that the absorbance curve of the product matched the blue diformazan of NBT (Marc & Sperling, 1976). The tissue curve was very similar to aqueous suspensions of NBT diformazan but with a red shift characteristic of diformazans in non-aqueous media (see Fig. 2).

Immunohistochemistry

Tissue blocks of six rats were selected for analysis. Two rats (rats 5 and 7, post surgery times 87 and 130 days) had undergone SC recording (see Table 1). The other four rats (200–256 days post surgery) did not undergo SC recording.

Blocks were sectioned into serial ultrathin datasets and probed with IgGs targeting L-glutamate, L-glutamine, glutathione, glycine, taurine, γ-aminobutyric acid (GABA) (Signature Immunologics Inc., Salt Lake City, UT, USA), rhodopsin rho1D-4 (a kind gift from Dr Robert Molday, University of British Columbia, Canada), LWS1 (red and green) cone opsin from Chemicon International Inc. (Temecula, CA, USA), and CRALBP (cellular retinaldehyde binding protein; a generous gift from Dr Jack Saari, University of Washington, Seattle, WA, USA), and DAPI (4′,6-diamidino-2-phenylindole dihydrochloride) (procedure after Marc & Jones, 2002).

CMP/data analysis

Computational molecular phenotyping has been extensively described in the literature (Marc *et al.*, 1995; Marc & Cameron, 2002; Marc & Jones, 2002). CMP fuses molecular and computational approaches to simultaneously visualize co-localized concentrations of small molecular species while preserving anatomical context at cellular resolution. Detection is accomplished with IgGs generated against epitopes of interest and the combination of signals defines individual cell classes. The immunocytochemistry is transformed into quantitative small molecular and protein signals along with cell anatomical data into multidimensional chemical signatures which can be segmented by classification algorithms to formally classify all cells into their ultimate, natural classes (Marc *et al.*, 1995; Marc & Jones, 2002).

In short, tissues taken post-fixation were dehydrated in a graded methanol series followed by acetone, then embedded in resin matrices as single specimens or stacks (Marc, 1999) followed by sectioning at 250 nm into serial arrays onto 12-well HTC® slides (Erie Scientific, Portsmouth, NH, USA). Sections of tissue were then probed with IgGs followed by probed CMP datasets being visualized with silver intensification (Marc *et al.*, 1990; Kalloniatis & Fletcher, 1993; Kalloniatis *et al.*, 1996) and counterstained with DAPI to show anatomy and simplify slice-to-slice registration. Images were captured in tiles at a calculated pixel scaling of 182 nm per pixel (40 × planapochromatic oil immersion lens) with a QImaging QICAM IEEE-1394 12-bit cooled monochrome camera (http://www.qimaging.com) capturing in 8-bits. Illumination was controlled with a regulated power supply. No filtering or contrast adjustment was used prior to image analysis. Images were co-registered with irTweak, developed at the University of Utah Scientific Computing Institute (http://www.sci.utah.edu/software.html) creating *n*-dimensional image

databases for subsequent quantitative analysis. Quantitative analysis of greyscale images with univariate histogramming and N-space cluster analysis was implemented as described in Marc *et al.* (1995) and Marc & Jones (2002). Our basic tool for univariate and multivariate histogram analysis is CellKit, an application developed in the Marc laboratory under the IDL image visualization language (http://www.rsinc.com), which operates in the freely distributed IDL VM environment. CellKit v2.2 is available from http://prometheus.med.utah.edu/~marclab/protocols_cellkit.html. Color images were assembled with Adobe Photoshop (San Jose, CA, USA). Complete protocols are available at http://prometheus.med.utah.edu/~marclab/protocols.html.

Statistical analysis of CMP data sets

In the analysis of sample sets, all CMP procedures were performed in a masked design. All samples were coded, and the assembly of sectioning arrays, performance of thin sectioning, immunoprobing and image capture were all executed by personnel with no knowledge of the sample identity or provenance. CMP is a high-precision quantitative method (Marc *et al.*, 1995; Marc & Cameron, 2002; Marc & Jones, 2002; Anderson *et al.*, 2009) allowing direct comparisons of small molecule concentrations and distributions within and across samples. The signal-to-noise ratio of CMP methods is such that the probability of the classification error (P_e) < 0.001 (Marc & Liu, 2000) for a single probe and the precision is high enough to discriminate 0.04 mM differences in a single probe across cell classes (Marc & Jones, 2002). The analysis of cell signatures (i.e. combinations of small molecules) to discriminate cell classes and characterize their states was performed by K-means clustering on silver density signals from registered serial sections (as described above) and the statistical separability expressed as P_e determined by transformed divergence. A detailed introduction to the use of clustering and divergence in immunocytochemistry is provided in reference (Marc & Cameron, 2002).

Quantification of neurotransmitter staining

Signature histograms from both transplant and host retinas were acquired for GABAergic and glycinergic amacrine cells using the methods established by (Marc & Jones, 2002). The histograms were converted to cumulative frequency distributions and compared by the Komolgorov–Smirnov (K-S) non-parametric statistic.

Results

SC responses

Visual responses to a full-field light stimulus could be recorded in transplanted rats in a restricted area of the SC corresponding to the placement of the transplant in the retina (Fig. 1B). Age-matched RD rats with sham surgery or cortical transplants showed no responses. An example is shown in Fig. 1. Visual response thresholds varied between −2.66 and −0.9 log cd/m^2 (see Table 1) with no clear correlation with transplant organization except that the rat with the least sensitive threshold contained a disorganized transplant.

Overview of statistical CMP results

In all cases described, the P_e (probability of classification error) of GABAergic amacrine cells, glycinergic amacrine cells, glutamatergic bipolar cells and glia was < 0.001. The discrimination of photoreceptors in transplant zones was absolute using the rhodopsin 1D4 monoclonal antibody, and P_e was not then computable; it was effectively 0. The key metrics in this study were the relative spatial distributions of cells and processes (bipolar cells, amacrine cells, glia) in defined transplant and host zones. Transplant zones were defined by three independent metrics: (i) regions with partial or complete outer nuclear laminations or rosettes and Rho 1D4 immunoreactivity, (ii) the presence of dual inner nuclear layers and (iii) regions harboring positive BCIP signals generated exclusively by the transplant. The correlation of these three signals was perfect across all 17 samples. Thus, the probability of incorrectly mapping the transplant zone in the n + 1th sample is < $1/(18)^3$ or 0.00017. All of the potential points of transplant GABAergic neurons fusing with the host retina occurred exclusively in these zones.

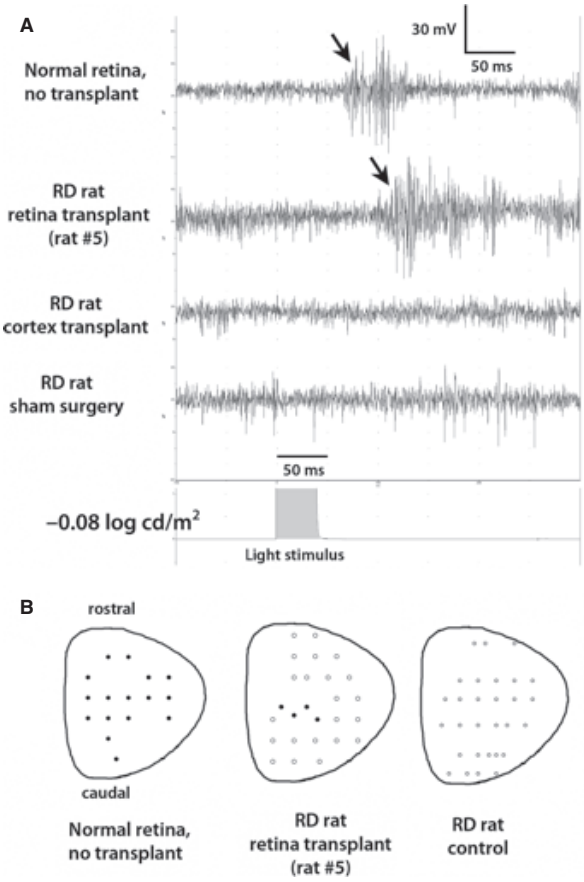

FIG. 1. Example of visual responses in the superior colliculus. (A) Response traces to a light stimulus of 0.08 log cd/m^2, starting at 100 ms before and ending 300 ms after start of a 40-ms full-field light stimulus. Recordings from a normal rat (without transplant), of RD rat no. 5 with transplant, an RD rat with cortex transplant and an RD sham surgery rat are shown. Arrows point to the onset of visual responses. There are no responses in the RD rat with cortex transplant or with sham surgery. Transplanted RD rat no. 5 shows a response delayed by approximately 30 ms compared with a normal rat. (B) Response maps of the right SC (oriented with rostral side up, caudal side down). Responses are indicated as black dots, non-responsive areas as circles. Normal rats have responses over the entire SC. In rat no. 5, a small area corresponding to the placement of the transplant in the retina shows visual responses whereas normal rats have responses over the entire SC and control RD rats (sham surgery, cortex transplant, non-surgery) have no responses. The response threshold of rat no. 5 was −2.66 log cd/m^2 (see Table 1).

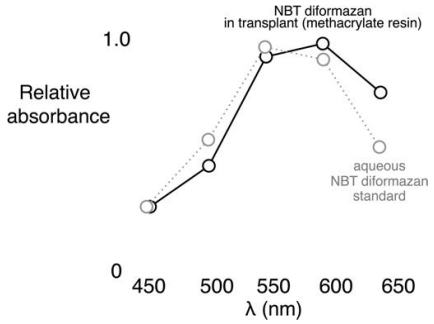

FIG. 2. Quantification of transplant-specific NBT staining. Absorbance of NBT reaction product vs. wavelength. Every retina was imaged in a spectral series at 400, 450, 500, 550, 600 and 650 nm to verify that the absorbance curve of the product matched the blue diformazan of NBT (Marc & Sperling, 1976). The tissue curve was then very similar to aqueous suspensions of NBT diformazan but with a red shift characteristic of diformazans in non-aqueous media. All the transplanted regions showed characteristic NBT diformazan densities ranging from 0.06 to 0.1 at 550 nm. This corresponds to an NBT diformazan concentration of ≈700 mM (using standard diformazan extinction coefficients and a section thickness of 200 nm), which is characteristic of diformazan reactions run to saturation. None of the host peripheral retinas from any of the samples showed any measurable density at any wavelength. They were absolutely transparent. Thus, the spectral absorbance data uniquely represent the presence of enzymatically reduced NBT. There is no intrinsic production of diformazan in the S344*ter* host retina. Diformazan is insoluble in aqueous media, ethanol and acetone and is non-diffusible. Thus, the reaction product in the IPL of S344*ter* host retina represents cellular elements from the transplanted retina entering the host. No diformazan is present in any nucleus, despite the immensely high concentration of product.

Transplant-specific NBT staining signals for hPAP in host IPL

In sections derived from hPAP-stained vibratome sections (example in Fig. 3A), all the transplanted regions showed characteristic NBT diformazan densities ranging from 0.06 to 0.1 at 550 nm. This corresponds to an NBT diformazan concentration of ≈700 mM (using standard diformazan extinction coefficients and a section thickness of 200 nm), which is characteristic of diformazan reactions run to saturation. None of the peripheral host retinas outside the transplant from any of the samples showed any measurable density at any wavelength. Thus, the spectral absorbance data (Fig. 2) uniquely represent the presence of enzymatically reduced NBT specific for the transplant. There is no intrinsic production of diformazan in the S344*ter* host retina. Furthermore, diformazan is insoluble in aqueous media, ethanol and acetone and is non-diffusible. Therefore, the reaction product in the IPL of S344*ter* host retina can conservatively only be interpreted as cellular elements from the transplanted retina entering the host. Further proof is that diformazan has a molecular weight of 749 Da and should readily diffuse into nuclei in the transplant region if it were diffusible. No diformazan was present in any nucleus, despite the immensely high concentration of product.

Figure 3 shows image processing of the BCIP/NBT diformazan signal. Proof of the unique distribution of the diformazan is provided in Fig. 3B, which is an RGB (red–green–blue) composite representing the spectral absorbance at 450 (blue channel), 500 (green channel) and 550 nm (red channel). This distinguishes NBT diformazan (blue) from melanin (brown). The host retina has no detectable signal. This is an unprocessed density image captured at a resolution of 364 nm per pixel. Figure 3C is the same image with a linear max–min contrast stretched from 8 down to 4 bits of data to reveal the shape of the infiltration region. Figure 3D shows Fig. 3B in combination with the autofluorescence image. Figure 3E is a green magenta map generated by inverting Fig. 3D and assigning it to the R + B channels and maintaining the autofluorescence as green.

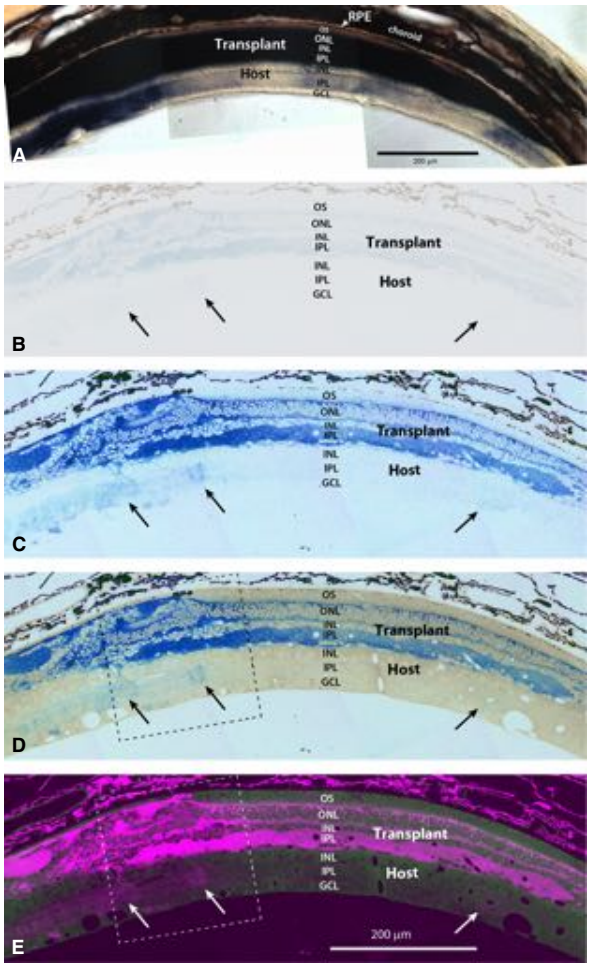

FIG. 3. hPAP-stained transplant (rat no. 7). Transplant with large area of lamination. (A) BCIP-stained 80-μm-thick vibratome slice. (B) Unprocessed density image of a 200-nm section captured at a resolution of 364 nm per pixel. This figure is an RGB composite representing the spectral absorbance at 450 (blue channel), 500 (green channel) and 550 nm (red channel). This distinguishes NBT diformazan (blue) from melanin (brown). The host retina is transparent and has no detectable signal. (C) Contrast-normalized nanometer density image – same image as A but linearly max–min contrast stretched from 8 down to 4 bits of data to reveal the shape of the infiltration region. (D) Image C with overlay of the autofluorescence image. (E) Magenta (fluorescence)/green (NBT signal) overlay – green magenta map generated by inverting D and assigning it to the R + B channels and maintaining the autofluorescence as green. Note the area of transplant process penetration into the host retina (arrows). Boxes in D and E indicate areas of enlargement in Fig. 4. In B–D, the right side of the images is tilted (deeper cut than the left side) with reduced staining (staining is strongest on the surface of the vibratome slice). Scale bars = 200 μm. INL, inner nuclear layer; IPL, inner plexiform layer; ONL, outer nuclear layer; OPL, outer plexiform layer; OS, outer segments; RPE, retinal pigment epithelium.

BCIP staining for hPAP identified the transplant (Figs 2–5) and indicated a very dense penetration of transplant processes into the IPL of the host retina (arrows in Fig. 3B–D), especially at the edges of laminated transplant areas, in the transition zone to more disorganized areas (Figs 3 and 4A and B). At the electron microscopy level, BCIP appeared as an irregular precipitate (Fig. 5) that densely filled the

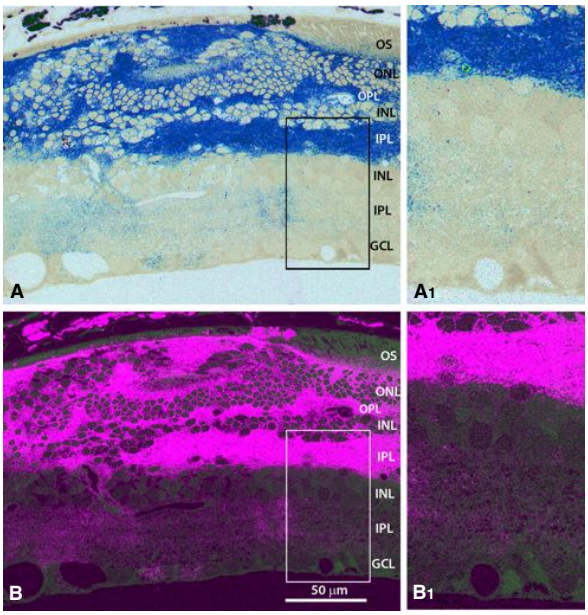

FIG. 4. Enlargements, showing penetration of transplant processes into the host IPL. (A) Enlargement of Fig. 3D. (B) Enlargement of Fig. 3E. Boxes show areas of further enlargement in A_1 and B_1. Punctate stain in the host IPL is visible at higher enlargement. Scale bar = 50 μm. INL, inner nuclear layer; IPL, inner plexiform layer; ONL, outer nuclear layer; OPL, outer plexiform layer; OS, outer segments.

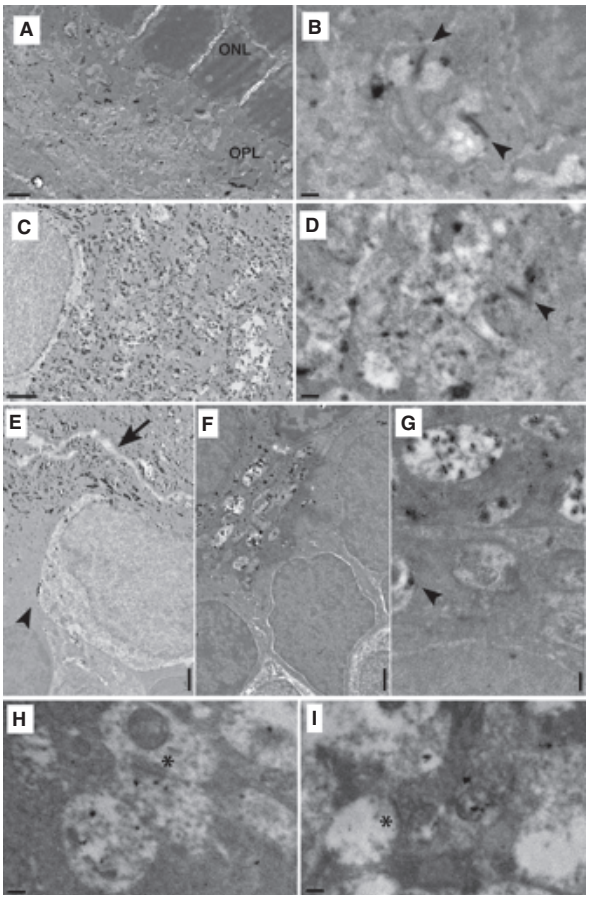

FIG. 5. Electron microscopy of BCIP donor stain. (A) Transplant outer plexiform and outer nuclear layers. Irregular BCIP precipitate in outer plexiform layer; no stain of nuclei; 10 seconds of uranyl acetate stain. (B) Enlargement of A, showing two triads in outer plexiform layer. Arrowheads point to ribbon synapses. BCIP seen as irregular precipitate. (C) Low magnification of transplant inner plexiform layer with BCIP stain. No counterstain. (D) High-magnification of a different area of the transplant inner plexiform layer. Arrowhead points to ribbon synapse. Ten seconds of uranyl acetate stain. (E) Transplant–host interface. Note that BCIP stain can be seen past a lighter appearing glial membrane (black arrow). No counterstain. (F) Transplant–host interface, different area in adjacent section. Ten seconds of uranyl acetate stain. (G) Enlargement of the transplant–host interface. Note stained process past transplant–host limit. Ten seconds of uranyl acetate stain. One BCIP-labeled process can be seen past the limit between transplant and host. (H,I) BCIP-labeled donor-derived processes in the host inner plexiform layer. Asterisks indicate unlabeled (presumable host) process in contact with BCIP-labeled (graft) process. No counterstain. A–G,I, rat no. 9; H, rat no. 7. Scale bars = 1 μm (A, C, E, F); 0.2 μm (B, D, G, H, I). ONL, outer nuclear layer; OPL, outer plexiform layer.

transplant areas (Fig. 5A–G). BCIP label was not found in nuclei. However, BCIP stain was only clear without counterstaining (Fig. 5C, E, H and I) or with very light counterstain (Fig. 5A, B, D, F and G). The staining mostly obscured synaptic structures in the transplant although ribbon synapses could occasionally be observed (Fig. 5B and D). BCIP-labeled processes could be identified in the host IPL (Fig. 5H and I).

Photoreceptors (rods and cones)

Transplant photoreceptors demonstrated strong taurine immunoreactivity (Fig. 6A, quantification in Fig. 7A). Rod and LWS (red-green opsin)-positive cone outer segments in contact with host RPE could only be found in the transplant region in laminated areas (Fig. 6B and C). Transplant photoreceptor outer segments interacted with host RPE (Fig. 6D–F). In disorganized transplant areas, there were clusters of survivor photoreceptors lacking outer segments (Fig. 8). No photoreceptors with inner and outer segments could be found in the host retina.

Quantification of neurotransmitter data

In no case were any significant differences in neurotransmitter level detectable between host and transplant (inner plexiform and inner nuclear layer) regions. For example, quantification of taurine levels (Fig. 7A) showed that host and transplant inner retinal layers contain indistinguishable taurine profiles due primarily to Müller and bipolar cells whereas the transplant photoreceptor layer contains extremely high taurine levels similar to the outer nuclear and outer segment layers of normal retina.

Figure 7B represents the frequency and cumulative distributions for GABA signals from host and transplant GABAergic amacrine cells from the same section. The histograms are statistically identical and the K-S statistic yields $P = 0.46$ (one-sided), which demonstrates that the distributions cannot be differentiated. Twelve comparisons were made and no transmitter showed a significant difference in level. Neuronal density was also assessed as the number of neurochemical cell types per unit length of IPL and no differences were found for GABAergic or glycinergic amacrine cells. For example, the dataset in Fig. 7B gives GABAergic amacrine cell density of 49/mm in the host and 52/mm in the transplant.

Glutamate signals were reliably higher in the transplant than the host and still higher in transplant areas without photoreceptors (Fig. 7C). The numbers of bipolar cells were similarly decreased in

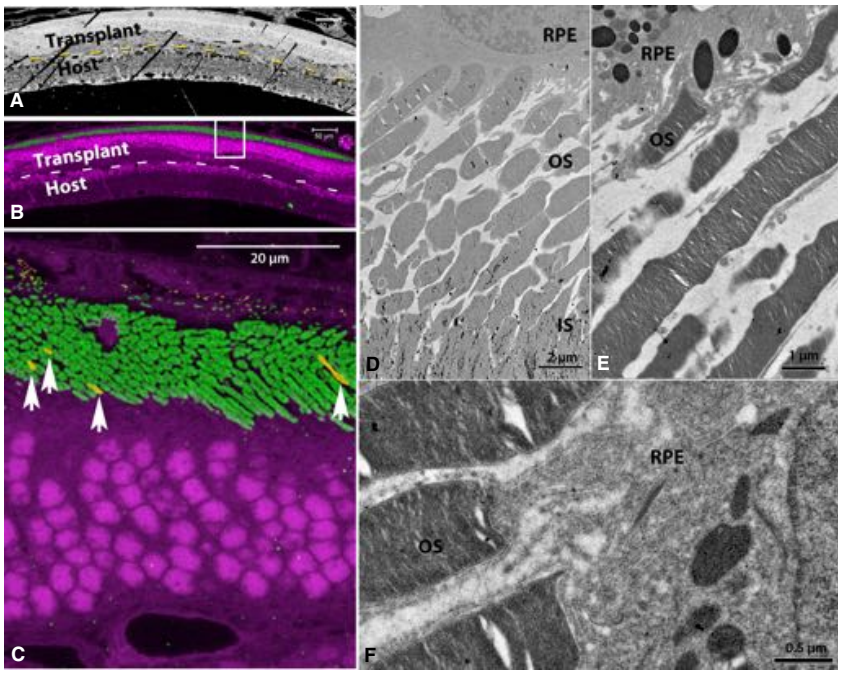

FIG. 6. Transplant photoreceptors (rods and cones). All images are oriented with the ganglion cell layer down. Rat no. 3. (A) Taurine – strong staining of transplant photoreceptors. Photoreceptor outer segments are indicated by asterisks (*). The inner retina of transplant and host both display normal taurine levels. Yellow dashes indicate approximate border between transplant and host. (B) Low-power micrograph. Rhodopsin staining of rod outer segments (green) can only be seen in the transplant region. DAPI-stained nuclei appear magenta. White dashes indicate approximate border between transplant and host. (C) Enlargement of white box in B; combination of rhodopsin (green), red–green opsin (orange) and DAPI (magenta). Arrows point to some cone outer segments among the dominant rod outer segments (only found in transplant area). (D) Electron micrograph of unstained ultrathin section of BCIP-stained block (rat no. 9), showing interaction between host RPE and transplant photoreceptor outer segments. BCIP can be seen as precipitate mainly in the inner segments. (E) Similar area in ultrathin section of rat no. 7, slightly counterstained with uranyl acetate. (F) Enlargement of adjacent area to D (rat no. 9, stained section). Transplant outer segments in contact with microvilli of host RPE. BCIP precipitate is difficult to see because of counterstain. Scale bars = 50 μm (A, B); = 20 μm (C); = 2 μm (D); = 1 μm (E) = 0.5 μm (F). IS, inner segments; OS, outer segments; RPE, retinal pigment epithelium.

both host and transplant compared with normal retina. The remnant inner nuclear layer was significantly more variable in thickness than normal rat (30–35 μm), ranging from 10 to 30 μm in both host and transplant. Given that the amacrine cell frequencies seem unaltered, most of the variation must have come from bipolar cell loss. However, there were still large clusters of bipolar cells, as evidenced by the high glutamate content of the host and transplant IPLs.

For reasons unknown, regions at the transplant edges that lost all photoreceptors demonstrated a much higher remnant neuronal glutamate content. In any case, the transplant regions always showed robust metabolic status to the host when photoreceptors were present.

Inner retinal neurons

The transplants maintained their correct lamination in the center of the transplant with altered topologies at the edges (example in Fig. 8). Both transplant and host displayed normal GABA, glutamate, glycine and glutathione levels in surviving bipolar, horizontal and amacrine cell classes (Figs 7–11), but extensive remodeling was found, especially at the transplant edges that had lost photoreceptors. The organized areas of the transplants with inner and outer segments showed the least remodeling, and showed plasticity in many areas of neuropil bridging between transplant and host (Fig. 10D and F).

Figure 8 shows a combination of glycine–DAPI–glutamate RGB mapping through the extent of a vibratome slice. The transplants appeared to maintain a relatively uniform thickness, but the transplant photoreceptor layer and inner nuclear layer thickness was inversely related to the IPL thickness. The transplant showed loss of inner retinal neurons, specifically bipolar cells. The inner nuclear layer of the transplant was overall thinner than that of the host (Fig. 9A). Areas of bridging between transplant–host neuropil was seen at the edges of laminated areas (Fig. 9B), and also in areas with two IPLs (Fig. 10E and G).

GABA staining (Fig. 10) showed extensive remodeling, especially at the transplant edges and in the host retina outside the transplant (Fig. 10C). Transplant and host displayed normal GABA levels (Fig. 7B). Although there were many areas with no or sparse mixing of transplant–host neuropil (examples in Fig. 10B and F), apparent mixing of transplant–host neuropil could be observed in the glycine, GABA and glutamate channels (Figs 9, and 10E and G).

Transplants contained many glutathione-immunoreactive horizontal cells (Fig. 11A) and there were usually more glycinergic amacrine cells in the laminated transplant area than in the degenerated host retina (Fig. 11B). Glutamate labeling (Figs 8, 9, and 11C and D) revealed areas of transplant photoreceptors and patches of rod nuclei within the transplant regions. Glutamate levels appeared normal in both the transplant and host inner retinas (slightly elevated in the transplant) (Fig. 7C), but as in glycine labeling, showed remodeling events by glutamatergic neuronal populations.

Glial cells

CRALBP was present at lower concentrations in the transplant zone with photoreceptors (Fig. 12A), but much stronger in the remodeled

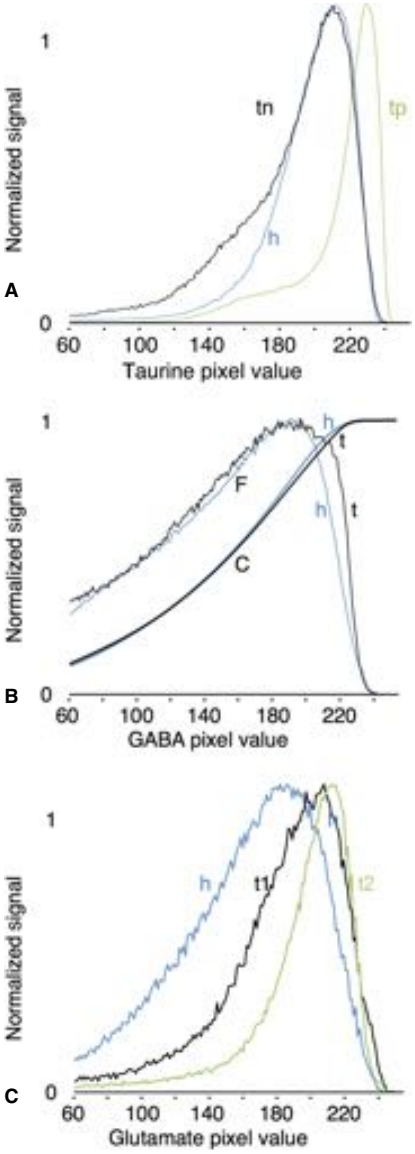

FIG. 7. Quantification of neurotransmitter data. (A) Normalized taurine pixel value probability frequency histograms for entire host retinal thickness (h, blue), transplant neural retina (tn, black) and transplant photoreceptor layer regions (tp, green), spanning over 2 mm of retina. Host and transplant neural retina contain indistinguishable taurine profiles due primarily to Müller and bipolar cells. The transplant photoreceptor layer contains extremely high taurine levels similar to the outer nuclear and outer segment layers of normal retina. (B) Normalized GABA pixel value probability frequency (F) and cumulative frequency (C) histograms for host (h, blue) and transplant (t, black) regions, spanning over 4.6 mm of retina and encompassing the entire host and transplant inner plexiform layer. The host contained 224 and the transplant 111 GABAergic amacrine cells. Normalized for inner plexiform layer length yields 49 and 52 amacrine cells/mm of inner plexiform layer length in the host and transplant, respectively. (C) Normalized glutamate pixel value probability frequency histograms for host (h, blue) and transplant regions with (t1, black) and without (t2, green) photoreceptors. Glutamate signals are reliably higher in the transplant than the host and much higher in transplanted retina without photoreceptors.

transplant zone (data not shown). A glial seal revealed by CRALBP and glutamine synthetase labeling was observed between the host and transplant retina (Fig. 12C and D). However, there were many regions

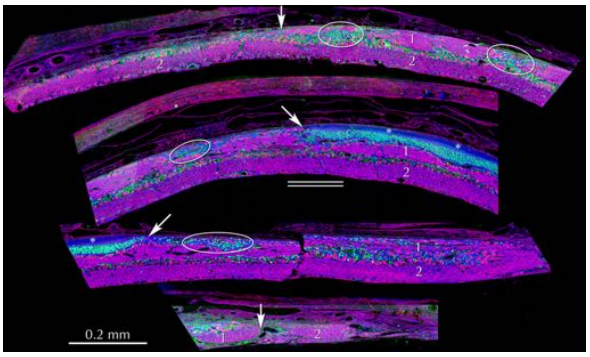

FIG. 8. Overview of transplant – glycine (red)–DAPI (green)–glutamate (blue) mapping. Rat no. 3. Glycine – subpopulation of amacrine cells; glutamate – rods and cones (≈ 1 mK), BCs, GCs (5–10 mM), ACs (0.04–1 mM), MCs (0.04–0.3 mM). Reduced version of a 300-Mb image that spans one vibratome slice over approximately 4.5 mm. It is digitally broken up into segments. This section does not contain the optic nerve. The vertical arrows indicate the transplant limits and the oblique arrows indicate the limit of intact outer segments (also indicated by asterisks *). Ovals indicate patches of rod nuclei (no outer segments). Numerals 1 and 2 denote the inner plexiform layers of the transplant and host, respectively. The double line indicates the region where Fig. 9A and B were taken. Scale bar = 0.2 mm.

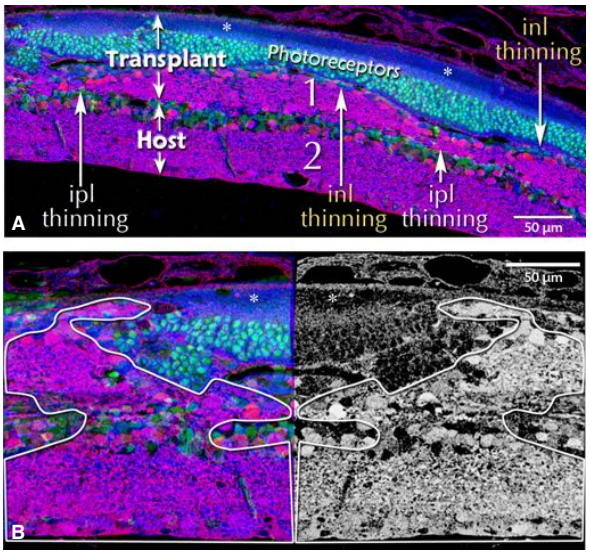

FIG. 9. Enlargements – glycine (red)–DAPI (green)–glutamate (blue). Two areas of Fig. 8, rat no. 3. Photoreceptor outer segments are indicated by asterisks (*). (A) Laminated area. Numerals 1 and 2 denote the inner plexiform layers of the transplant and host, respectively. The inner nuclear layer of the transplant is overall thinner than that of the host. It appears still thinner in areas where the inner plexiform layer of the transplant is thicker, and *vice versa*. (B) Higher magnification view of the underlined region in Fig. 8, at the edge on the laminated area. The left RGB image is mirrored by the right glycine channel alone (intensity mapped like fluorescence). The transplant–host neuropil is mixed all the way from the microneuroma at the top, though the transplant, into the host. Scale bars = 50 μm.

where the seal was clearly absent, revealing areas of bridging between host and transplant retinas (detail shown in Fig. 12B_1 and C_1).

Additionally, transplant and host both displayed normal glutamine levels, but glial glutamine levels were elevated in the remodeled zones at the transplant edges and in the host retina outside the transplant (data not shown).

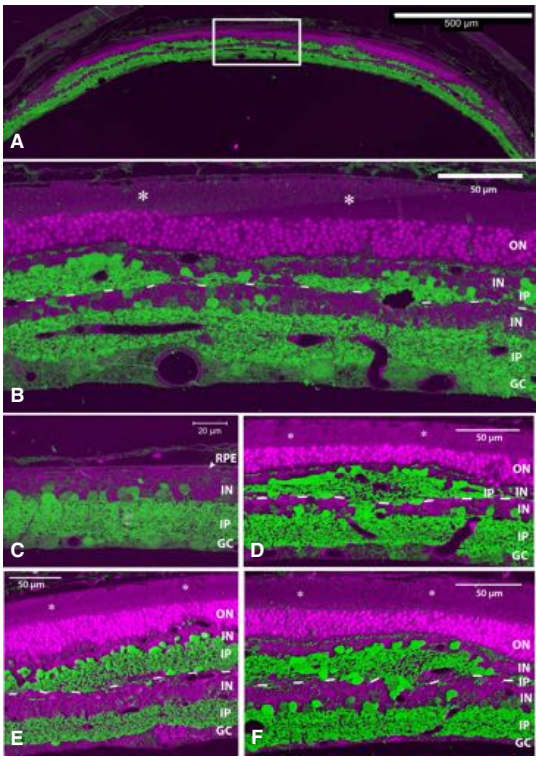

FIG. 10. GABA-ergic amacrine cells. GABA – green, DAPI (nuclei) – magenta. Dashes indicate approximate transplant–host border. (A,B) Rat no. 1. Photoreceptor outer segments are indicated by asterisks (*). (A) Overview. GABA stain reveals remodeling, especially in areas with photoreceptor loss at the edge (not shown) and outside the transplant. Area of enlargement is indicated by white box. (B) Enlargement of transplant. (C) Host retina outside transplant area, rat no. 2. No outer nuclear layer. (D) Rat no. 1, different slice than in A,B. Clear process mixing and fusion of migration columns. E) Rat no. 2. No obvious mixing. (F) Different slice of rat no. 2 with transplant GABA neurons remodeling (migrating) into the host zone. Scale bars = 500 μm (A); 50 μm (B, D, E, F); 20 μm (C). INL, inner nuclear layer; IPL, inner plexiform layer; ONL, outer nuclear layer; OPL, outer plexiform layer; OS, outer segments; RPE, retinal pigment epithelium.

Discussion

After transplantation to retinal degeneration models using a gentle transplantation method, fetal retinal sheet transplants have been shown to develop retinal layers and then retain their lamination, including photoreceptor outer segments (Seiler & Aramant, 1998), to form synaptic connections with the host (Seiler *et al.*, 2008c, 2010) and to restore visual responses in the SC (Sagdullaev *et al.*, 2003; Thomas *et al.*, 2004; Yang *et al.*, 2010). CMP has uniquely revealed the rearrangement of retinal topology and demonstrated circuit revision (retinal remodeling) in photoreceptor degenerations (Marc & Jones, 2003; Marc *et al.*, 2003, 2007; Jones & Marc, 2005; Marc, 2010). This study sought to implement CMP (Marc *et al.*, 1995; Marc & Jones, 2002) to visualize cell classes and to examine potential circuitries involved in fetal retinal sheet transplants.

Visual responses in the SC

Electrophysiological recording from the SC was used to provide additional information about the function of the transplants. In normal rats, responses were found all over the SC at different light intensities down to −5 log cd/m^2. No visual responses could be recorded in age-matched degenerate RD retina controls at the tested light levels of −0.08 to −3.5 log cd/m^2 whereas responses with longer response latencies were found in transplanted rats in a small area corresponding to the placement of the transplant in the host retina. Visual thresholds varied between transplanted rats. The mechanism of restoration of visual function has been explained as a rescue effect of the transplant on host cones by some research groups. For example, MacLaren & Pearson (2007) stated that visual responses in transplanted rats could be explained by a mere rescue effect of host cones. However, previous research has shown (Sagdullaev *et al.*, 2003; Thomas *et al.*, 2004; Seiler *et al.*, 2008b,c, 2010) that it is not a rescue effect, although a beneficial trophic effect of the developing fetal transplant on the host is probably involved. After retinal sheet transplantation in this S334*ter* line 3 rat model, there was no difference in the distribution of red–green opsin-immunoreactive cones in the host retina over the transplant area compared with outside the transplant whereas visual responses in the SC were limited to areas that topographically corresponded to the transplant position in the host retina (Seiler *et al.*, 2008b). In addition, we have demonstrated that the degree of trans-synaptic labeling of the transplants from the SC is correlated with the visual threshold in SC recordings (Seiler *et al.*, 2008c), and that transplants extend neuronal processes into the IPL of the host retina and form synapses with host cells (Seiler *et al.*, 2010).

Photoreceptors

In all examined samples, cell survival and retinal remodeling appeared in a mosaicked fashion with the transplant containing areas of healthy rods and cones whereas the photoreceptors in the host retina were degenerated at the time points observed. Cone opsin immunoreactivity in the transplants was similar to normal rats while rod or cone opsin in the host retina was not observed. Other studies have shown surviving host cones using red–green opsin (Seiler *et al.*, 2008b; Yang *et al.*, 2010) or S-antigen/arrestin immunohistochemistry (Sagdullaev *et al.*, 2003). Although S334*ter* line 3 rats never develop rod outer segments (Liu *et al.*, 1999), cone outer segments – labeled with peanut agglutinin – are found over the whole retina at P10, diminish at P20–30 and are reduced to isolated spots at P60–90 (Li *et al.*, 2010; Martinez-Navarrete *et al.*, 2011). At P180, S-opsin-immunoreactive cones show amacrine cell-like morphology and entirely lack outer segments (Hombrebueno *et al.*, 2010).

The current study implies that degenerating host cones are not capable of any light response. Correspondingly, visual responses in the SC were restricted to an area corresponding to the placement of the transplant in the retina, confirming previous studies (Sagdullaev *et al.*, 2003; Seiler *et al.*, 2008b; Yang *et al.*, 2010).

Bipolar cells

In every sample, fewer inner retinal neurons were found in the transplants compared with the adjacent host. There appeared to be an inverse relationship between the thickness of the transplant photoreceptor layer and the transplant IPL.

In the host and to a lesser extent in the transplant, an extensive loss of inner retinal neurons, specifically bipolar cells (BCs), was observed. More than 90% of the cells in the transplant inner nuclear layer consisted of amacrine cells (ACs) and Müller cells (MCs). In the normal retina, the inner nuclear layer contains more bipolar than amacrine and Müller cells together (BCs > MCs = ACs) (Jeon *et al.*, 1998).

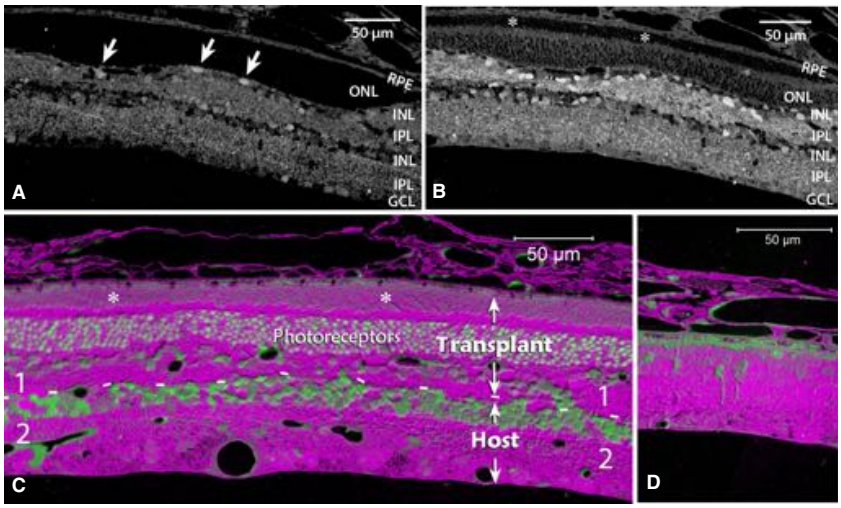

FIG. 11. Glutathione, glycine, glutamate. Photoreceptor outer segments are indicated by asterisks (*). (A,B) Rat no. 3. (A) Glutathione – the transplant and host both display normal glutathione levels in the inner plexiform layers, but are remodeled. Notably, the transplant has high glutathione + survivor horizontal cells at the OPL/ONL border (arrows). Few stained cells in host in this area. (B) Adjacent area – glycine immunoreactivity in laminated area with outer segments (*). This area appears to contain more glycinergic cells in the transplant than in the host. (C,D) Rat no. 1. Glutamate – magenta, DAPI – green. (C) Laminated area with outer segments (*). Normal glutamate levels in transplant and host, but remodeling. Dashes indicate approximate transplant–host border. (D) Host retina outside the zone of transplant. Scale bars = 50 µm. INL, inner nuclear layer; IPL, inner plexiform layer; ONL, outer nuclear layer; OPL, outer plexiform layer; RPE, retinal pigment epithelium.

Bipolar cells were probably lost in host and graft due to cell death (Marc *et al.*, 2003; Ray *et al.*, 2010), or they did not properly develop in the transplant (as in a Chx−/− mouse) (Livne-Bar *et al.*, 2006).

In S334*ter* line 3 rats, a significant reduction (50–75%) of rod BCs has been observed at ages P60–90 (Ray *et al.*, 2010). Similar to other retinal degeneration models (Jones *et al.*, 2003; Marc & Jones, 2003; Peng *et al.*, 2003; Cuenca *et al.*, 2004; Strettoi *et al.*, 2004), rod BCs in S334*ter* line 3 rats respond to photoreceptor loss with abnormal sprouting and ectopic synapses (Ray *et al.*, 2010). However, numerous rod BCs have been shown by protein kinase C alpha and mGluR6 immunohistochemistry in fetal retinal sheet transplants (e.g. Seiler *et al.*, 2008b). As the total number of BCs was reduced with probably no loss in rod BCs, this indicates a specific loss of cone BCs in the transplant inner nuclear layer. It corresponds to unpublished data indicating that transplants contain few recoverin-immunoreactive cone bipolar cells. This will need to be further explored as the current study was not designed to solve this issue.

At the time of transplantation (E19), the donor tissue consisted mostly of retinal progenitor cells, except for ganglion cells, cones, some amacrine and horizontal cells (Uesugi *et al.*, 1992; Alexiades & Cepko, 1997). Rods and rod BCs are derived from the same progenitor (Turner & Cepko, 1987), and compete for their cell fate choice (Brzezinski *et al.*, 2010), which can occur after the final mitosis (Belliveau *et al.*, 2000). The bHLH genes *Mash1* and *Math3*, and the homeobox gene *Chx10/Vsx2* are essential for generation of bipolar cells (Hatakeyama *et al.*, 2001). The degenerating host retina may present a different environment for the retinal progenitor cells in the transplant than a normally developing fetal retina.

Glial seal

Photoreceptor degeneration is accompanied by extensive hypertrophy of MCs and development of glial seals (Jones *et al.*, 2003).

It has been postulated that retinal transplants cannot integrate with the host retina because of a glial seal between transplant and host which needs to be disrupted for any connectivity to occur (Suzuki *et al.*, 2007; West *et al.*, 2008). However, the current study confirms that fetal retinal sheet transplants can 'integrate' with a degenerating host retina, in areas lacking a glial barrier between transplant and host (e.g. Seiler & Aramant, 1998; Seiler *et al.*, 2010). The transplants were performed at a time when all host rod photoreceptors were lost, but still at an early stage of degeneration. The absence of the glial seal could be due to the influence of the developing transplant to inhibit the development of a glial seal formation or to disruption of the outer limiting membrane due to the surgery. The BCIP staining for the donor cell label indicated that transplants extended processes into the host retina, confirming previous studies (Seiler *et al.*, 2010).

In addition, novel connectivity between a degenerating retinal host and an embryonic transplant may depend on the model of retinal degeneration as transplants to *rd* mice demonstrated less host/transplant integration (Arai *et al.*, 2004). In subretinal transplants to normal retinas or to slow retinal degenerative models, the outer limiting membrane surrounding photoreceptors may function as a barrier for transplant host integration (Zhang *et al.*, 2003).

Remodeling

Early in retinal degenerations, bipolar cells retract dendrites from the photoreceptor terminals and subsequently form polyaxonal processes that sprout into the outer nuclear layer and potentially also into the IPL. These bipolar cell processes also contribute to the formation of new neuropil along with amacrine and horizontal cells (Jones & Marc, 2005). These new processes could also be responsible for the integration of neuropil between host and transplant, and for the IPL demonstrated in the distorted IPL images of the transplant in this study.

Retinal remodeling of the transplant was more pronounced than that of the host retina with apparent neovascularization outside the photoreceptor layer. Retinal remodeling represents the likely recapitulation of mechanisms that resemble development and plasticities seen elsewhere in the central nervous system (Jones & Marc, 2005;

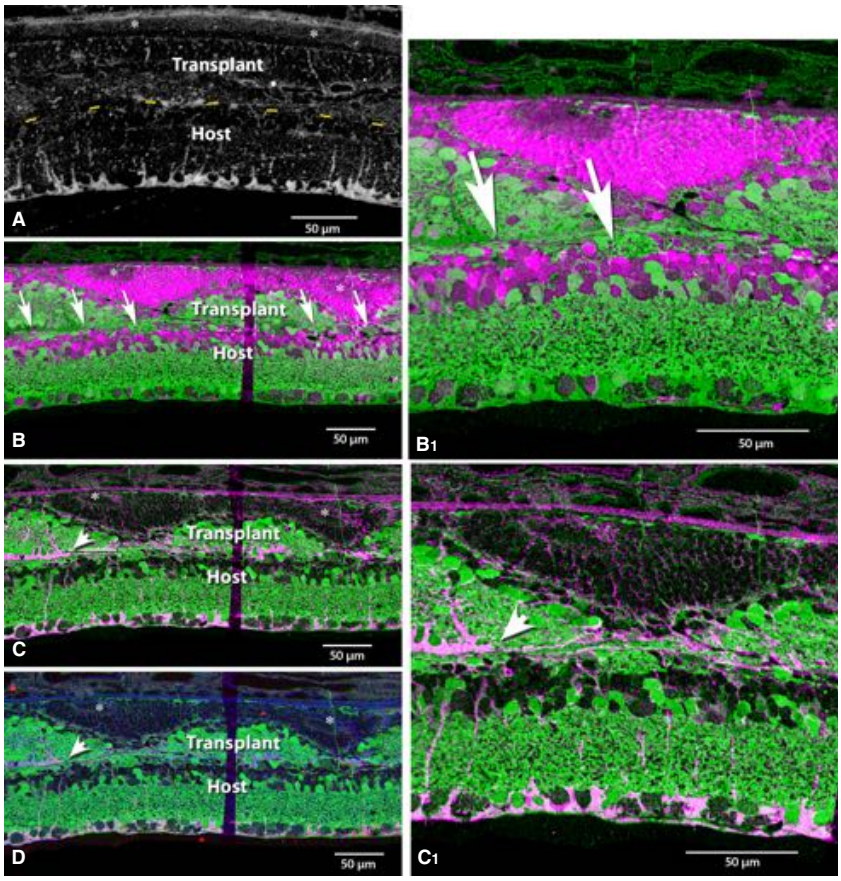

FIG. 12. Glial markers – areas without inner limiting membrane between transplant and host. Asterisks (*) indicate presence of outer segments. (A) Rat no. 3. CRALBP (marker for Müller glia and RPE) is present but less expressed in the transplant area with photoreceptors. CRALBP is much stronger in the remodeled, more disorganized transplant areas (not shown on this picture). (B–D) Rat no. 5. Transplant area showing some disorganization, imaged with combinations of GABA staining (green) with various other labels. (B) DAPI – magenta. Arrows indicate transplant–host interface. (B_1) Enlargement. (C) CRALBP – magenta. (C_1) Enlargement. (D) CRALBP – red; glutamine synthetase (GS) – blue. Glial seal on left side (arrowhead in C and D) is interrupted through most of the area, with neural processes crossing the transplant–host interface. Scale bars = 50 μm.

Draguhn *et al.*, 2008). It had previously been hypothesized that retinal transplants would also remodel (Jones & Marc, 2005; Jones *et al.*, 2005; Marc *et al.*, 2005), but that there were no mechanisms in place to establish communication between transplanted retina and the degenerating host retina. Indeed, the concern was also that there were no mechanisms in place to prevent transplant remodeling. However, this study demonstrates that plasticity-like phenomena could serve as a means for retinal transplant integration into the host retina. Neurons within the host and transplant retinas appear to represent healthy cell populations and it may be possible to influence their emergent rewiring and cellular migration to guide future transplant integrations.

The current study could not establish whether there were any differences between the BDNF and GDNF treatment of the transplants due to the low N and transplant variability. A more detailed analysis of transplant functional effects after BDNF or GDNF treatment has been published by Yang *et al.* (2010).

Novel non-canonical circuitry

Given that this is a rodent model, cone BCs are rare in both the host and the transplant. In spite of cone bipolar cell loss in the transplant, there were still more cone BCs in the transplant than in the host along with substantial populations of surviving horizontal cells visualized with glutathione immunoreactivity. This finding, along with previous results (data not shown), suggests that horizontal cells contribute substantially to retinal remodeling and may represent a target for study and intervention with fetal transplants. Other obvious contributors demonstrated by the glycine and GABA channels (Figs 9–11) suggest that any major communication between the host and transplant is likely to involve horizontal and both glycinergic and GABAergic ACs.

The data confirm studies of trans-synaptic tracing (Seiler *et al.*, 2005, 2008c) and identification of donor-derived synapses in the host IPL (Seiler *et al.*, 2010), demonstrating that synaptic connectivity between transplant and host contributes to restoration of visual responses in the SC. Further study is required to determine the retinal circuit topology between host and transplant retinas. However, this knowledge will be dependent upon a more complete understanding of normal retinal circuitry, which is currently grossly limited (Anderson *et al.*, 2009, 2011).

Conclusions

At the time of examination (about 4–10 months after transplantation), retinal progenitor sheet transplants contained regions of healthy rods

and cones superimposed upon rod/cone degeneration in the host retina. Extensive loss of neurons, including BCs, was observed in the transplant inner nuclear layer although remaining cell populations appeared healthy. Frequently, host and transplant neuropil had become mixed where glial barriers were missing. Horizontal cells, and both glycinergic and GABAergic ACs are probably involved in bridging connectivities between transplant and host, potentially creating alternative signaling pathways. Although these studies give substantial support to vision therapy strategies involving sheets of retinal progenitor cells, more work is needed to define transplant/host integration in retinal degenerative disease.

Acknowledgements

This research was supported by the Lincy Foundation (M.J.S., R.B.A., H.S.K.), NIH Grants EY02576 (R.E.M.), EY015128, EB005832 (R.E.M.), EY014800 Vision Core (R.E.M.), Research to Prevent Blindness Career Development Award (B.W.J.), Edward N. and Della L. Thome Memorial Foundation grant for Age-Related Macular Degeneration Research (B.W.J.). The funders had no role in study design, data collection and analysis, decision to publish, or preparation of the manuscript. The technical assistance of Fengrong Yan, Lakshmi Patil, Ilse Sears-Kraxberger (UC Irvine), and Margurite V. Shaw and Jia Hui Yang (University of Utah) is appreciated. We also thank Drs Biju Thomas (Doheny Eye Institute, Los Angeles) and Leonard Kitzes (Department of Anatomy & Neurobiology, UC Irvine) for their help with the electrophysiology setup. M.J.S. and R.B.A. have proprietary interests in the implantation instrument and procedure (Ocular Transplantation LLC; patents no. 5,941,250; 6,159,218; 6,156,042); R.B.A. is also an employee of Ocular Transplantation LLC. H.S.K. is on the scientific advisory board of California Stem Cell Inc., and R.E.M. has proprietary interests in Signature Immunologics Inc.

Abbreviations

AC, amacrine cell; BC, bipolar cell; BCIP, 5-bromo-4-chloro-3-indolyl phosphate (alkaline phosphatase substrate); BDNF, brain-derived neurotrophic factor; CMP, computational molecular phenotyping; CRALBP, cellular retinaldehyde binding protein; DAPI, 4′,6-diamidino-2-phenylindole dihydrochloride; GABA, gamma-aminobutyric acid; GDNF, glial cell-derived neurotrophic factor; hPAP, human placental alkaline phosphatase (donor label); IPL, inner plexiform layer; MC, Müller cell; NBT, nitro blue tetrazolium chloride (alkaline phosphatase substrate); RD, retinal degenerate or retinal degeneration; RGB, red–green–blue; RPE, retinal pigment epithelium; SC, superior colliculus.

References

Alexiades, M.R. & Cepko, C.L. (1997) Subsets of retinal progenitors display temporally regulated and distinct biases in the fates of their progeny. *Development*, **124**, 1119–1131.

Anderson, J.R., Jones, B.W., Yang, J.H., Shaw, M.V., Watt, C.B., Koshevoy, P., Spaltenstein, J., Jurrus, E., U.V., K., Whitaker, R.T., Mastronarde, D., Tasdizen, T. & Marc, R.E. (2009) A computational framework for ultrastructural mapping of neural circuitry. *PLoS Biol.*, **7**, e1000074.

Anderson, J.R., Jones, B.W., Watt, C.B., Shaw, M.V., Yang, J.-H., DeMill, D., Lauritzen, J.S., Lin, Y., Rapp, K.D., Mastronarde, D., Koshevoy, P., Grimm, B., Tasdizen, T., Whitaker, R. & Marc, R.E. (2011) Exploring the retinal connectome. *Mol. Vis.*, **17**, 355–379.

Arai, S., Thomas, B.B., Seiler, M.J., Aramant, R.B., Qiu, G., Mui, C., de Juan, E. & Sadda, S.R. (2004) Restoration of visual responses following transplantation of intact retinal sheets in rd mice. *Exp. Eye Res.*, **79**, 331–341.

Aramant, R.B. & Seiler, M.J. (2002) Retinal transplantation – advantages of intact fetal sheets. *Prog. Retin. Eye Res.*, **21**, 57–73.

Aramant, R.B. & Seiler, M.J. (2004) Progress in retinal sheet transplantation. *Prog. Retin. Eye Res.*, **23**, 475–494.

Belliveau, M.J., Young, T.L. & Cepko, C.L. (2000) Late retinal progenitor cells show intrinsic limitations in the production of cell types and the kinetics of opsin synthesis. *J. Neurosci.*, **20**, 2247–2254.

Berson, E.L., Rosner, B., Weigel-DiFranco, C., Dryja, T.P. & Sandberg, M.A. (2002) Disease progression in patients with dominant retinitis pigmentosa and rhodopsin mutations. *Invest. Ophthalmol. Vis. Sci.*, **43**, 3027–3036.

Brzezinski, J.A., Lamba, D.A. & Reh, T.A. (2010) Blimp1 controls photoreceptor versus bipolar cell fate choice during retinal development. *Development*, **137**, 619–629.

Cuenca, N., Pinilla, I., Sauve, Y., Lu, B., Wang, S. & Lund, R.D. (2004) Regressive and reactive changes in the connectivity patterns of rod and cone pathways of P23H transgenic rat retina. *Neuroscience*, **127**, 301–317.

Draguhn, A., Axmacher, N. & Kolbaev, S. (2008) Presynaptic ionotropic GABA receptors. *Results Probl. Cell Differ.*, **44**, 69–85.

Gouras, P. & Tanabe, T. (2003) Survival and integration of neural retinal transplants in rd mice. *Graefes Arch. Clin. Exp. Ophthalmol.*, **241**, 403–409.

Green, E.S., Menz, M.D., LaVail, M.M. & Flannery, J.G. (2000) Characterization of rhodopsin mis-sorting and constitutive activation in a transgenic rat model of retinitis pigmentosa. *Invest. Ophthalmol. Vis. Sci.*, **41**, 1546–1553.

Hatakeyama, J., Tomita, K., Inoue, T. & Kageyama, R. (2001) Roles of homeobox and bHLH genes in specification of a retinal cell type. *Development*, **128**, 1313–1322.

Hombrebueno, J.R., Tsai, M.M., Kim, H.L., De Juan, J., Grzywacz, N.M. & Lee, E.J. (2010) Morphological changes of short-wavelength cones in the developing S334ter-3 transgenic rat. *Brain Res.*, **1321**, 60–66.

Jensen, R.J. & Rizzo, J.F. III (2009) Activation of ganglion cells in wild-type and rd1 mouse retinas with monophasic and biphasic current pulses. *J. Neural Eng.*, **6**, 035004.

Jeon, C.J., Strettoi, E. & Masland, R.H. (1998) The major cell populations of the mouse retina. *J. Neurosci.*, **18**, 8936–8946.

Jones, B.W. & Marc, R.E. (2005) Retinal remodeling during retinal degeneration. *Exp. Eye Res.*, **81**, 123–137.

Jones, B.W., Watt, C.B., Frederick, J.M., Baehr, W., Chen, C.K., Levine, E.M., Milam, A.H., LaVail, M.M. & Marc, R.E. (2003) Retinal remodeling triggered by photoreceptor degenerations. *J. Comp. Neurol.*, **464**, 1–16.

Jones, B.W., Watt, C.B. & Marc, R.E. (2005) Retinal remodelling. *Clin. Exp. Optom.*, **88**, 282–291.

Kalloniatis, M. & Fletcher, E.L. (1993) Immunocytochemical localization of the amino acid neurotransmitters in the chicken retina. *J. Comp. Neurol.*, **336**, 174–193.

Kalloniatis, M., Marc, R.E. & Murry, R.F. (1996) Amino acid signatures in the primate retina. *J. Neurosci.*, **16**, 6807–6829.

Kisseberth, W.C., Brettingen, N.T., Lohse, J.K. & Sandgren, E.P. (1999) Ubiquitous expression of marker transgenes in mice and rats. *Dev. Biol.*, **214**, 128–138.

Kolomiets, B., Dubus, E., Simonutti, M., Rosolen, S., Sahel, J.A. & Picaud, S. (2010) Late histological and functional changes in the P23H rat retina after photoreceptor loss. *Neurobiol. Dis.*, **38**, 47–58.

Lee, E.S. & Flannery, J.G. (2007) Transport of truncated rhodopsin and its effects on rod function and degeneration. *Invest. Ophthalmol. Vis. Sci.*, **48**, 2868–2876.

Li, Y., Tao, W., Luo, L., Huang, D., Kauper, K., Stabila, P., LaVail, M.M., Laties, A.M. & Wen, R. (2010) CNTF induces regeneration of cone outer segments in a rat model of retinal degeneration. *PLoS ONE*, **5**, e9495.

Lin, J.H. & LaVail, M.M. (2010) Misfolded proteins and retinal dystrophies. *Adv. Exp. Med. Biol.*, **664**, 115–121.

Lin, B., Masland, R.H. & Strettoi, E. (2009) Remodeling of cone photoreceptor cells after rod degeneration in rd mice. *Exp. Eye Res.*, **88**, 589–599.

Liu, C., Li, Y., Peng, M., Laties, A.M. & Wen, R. (1999) Activation of caspase-3 in the retina of transgenic rats with the rhodopsin mutation s334ter during photoreceptor degeneration. *J. Neurosci.*, **19**, 4778–4785.

Livne-Bar, I., Pacal, M., Cheung, M.C., Hankin, M., Trogadis, J., Chen, D., Dorval, K.M. & Bremner, R. (2006) Chx10 is required to block photoreceptor differentiation but is dispensable for progenitor proliferation in the postnatal retina. *Proc. Natl. Acad. Sci. U.S.A.*, **103**, 4988–4993.

MacLaren, R.E. & Pearson, R.A. (2007) Stem cell therapy and the retina. *Eye*, **21**, 1352–1359.

Mansergh, F.C., Vawda, R., Millington-Ward, S., Kenna, P.F., Haas, J., Gallagher, C., Wilson, J.H., Humphries, P., Ader, M. & Farrar, G.J. (2010) Loss of photoreceptor potential from retinal progenitor cell cultures, despite improvements in survival. *Exp. Eye Res.*, **91**, 500–512.

Marc, R.E. (1999) Kainate activation of horizontal, bipolar, amacrine, and ganglion cells in the rabbit retina. *J. Comp. Neurol.*, **407**, 65–76.

Marc, R.E. 2010. Injury and repair: retinal remodeling. In Besharse, J. & Bok, D. (Eds), *Encyclopedia of the Eye*. Elsevier, Amsterdam, pp. 414–420.

Marc, R.E. & Cameron, D. (2002) A molecular phenotype atlas of the zebrafish retina. *J. Neurocytol.*, **30**, 593–654.

Marc, R.E. & Jones, B.W. (2002) Molecular phenotyping of retinal ganglion cells. *J. Neurosci.*, **22**, 413–427.

Marc, R.E. & Jones, B.W. (2003) Retinal remodeling in inherited photoreceptor degenerations. *Mol. Neurobiol.*, **28**, 139–147.
Marc, R.E. & Liu, W. (2000) Fundamental GABAergic amacrine cell circuitries in the retina: nested feedback, concatenated inhibition, and axosomatic synapses. *J. Comp. Neurol.*, **425**, 560–582.
Marc, R. & Sperling, H. (1976) The chromatic organization of the goldfish cone mosaic. *Vision. Res.*, **16**, 1211–1224.
Marc, R.E., Liu, W.L., Kalloniatis, M., Raiguel, S.F. & van Haesendonck, E. (1990) Patterns of glutamate immunoreactivity in the goldfish retina. *J. Neurosci.*, **10**, 4006–4034.
Marc, R.E., Murry, R.F. & Basinger, S.F. (1995) Pattern recognition of amino acid signatures in retinal neurons. *J. Neurosci.*, **15**, 5106–5129.
Marc, R.E., Jones, B.W., Watt, C.B. & Strettoi, E. (2003) Neural remodeling in retinal degeneration. *Prog. Retin. Eye Res.*, **22**, 607–655.
Marc, R.E., Kalloniatis, M. & Jones, B.W. (2005) Excitation mapping with the organic cation AGB2+. *Vision. Res.*, **45**, 3454–3468.
Marc, R.E., Jones, B.W., Anderson, J.R., Kinard, K., Marshak, D.W., Wilson, J.H., Wensel, T. & Lucas, R.J. (2007) Neural reprogramming in retinal degeneration. *Invest. Ophthalmol. Vis. Sci.*, **48**, 3364–3371.
Marc, R.E., Jones, B.W., Watt, C.B., Vazquez-Chona, F., Vaughan, D.K. & Organisciak, D.T. (2008) Extreme retinal remodeling triggered by light damage: implications for age related macular degeneration. *Mol. Vis.*, **14**, 782–806.
Margolis, D.J., Newkirk, G., Euler, T. & Detwiler, P.B. (2008) Functional stability of retinal ganglion cells after degeneration-induced changes in synaptic input. *J. Neurosci.*, **28**, 6526–6536.
Martinez-Navarrete, G., Seiler, M.J., Aramant, R.B., Fernandez-Sanchez, L., Pinilla, I. & Cuenca, N. (2011) Retinal degeneration in two lines of transgenic S334ter rats. *Exp. Eye Res.*, **92**, 227–237.
Mujtaba, T., Han, S.S., Fischer, I., Sandgren, E.P. & Rao, M.S. (2002) Stable expression of the alkaline phosphatase marker gene by neural cells in culture and after transplantation into the CNS using cells derived from a transgenic rat. *Exp. Neurol.*, **174**, 48–57.
Peng, Y.W., Senda, T., Hao, Y., Matsuno, K. & Wong, F. (2003) Ectopic synaptogenesis during retinal degeneration in the Royal College of Surgeons rat. *Neuroscience*, **119**, 813–820.
Radtke, N.D., Aramant, R.B., Petry, H.M., Green, P.T., Pidwell, D.J. & Seiler, M.J. (2008) Vision improvement in retinal degeneration patients by implantation of retina together with retinal pigment epithelium. *Am. J. Ophthalmol.*, **146**, 172–182.
Ray, A., Sun, G.J., Chan, L., Grzywacz, N.M., Weiland, J. & Lee, E.J. (2010) Morphological alterations in retinal neurons in the S334ter-line3 transgenic rat. *Cell Tissue Res.*, **339**, 481–491.
Sagdullaev, B.T., Aramant, R.B., Seiler, M.J., Woch, G. & McCall, M.A. (2003) Retinal transplantation-induced recovery of retinotectal visual function in a rodent model of retinitis pigmentosa. *Invest. Ophthalmol. Vis. Sci.*, **44**, 1686–1695.
Sauvé, Y., Klassen, H., Whiteley, S.J. & Lund, R.D. (1998) Visual field loss in RCS rats and the effect of RPE cell transplantation. *Exp. Neurol.*, **152**, 243–250.
Seiler, M.J. & Aramant, R.B. (1998) Intact sheets of fetal retina transplanted to restore damaged rat retinas. *Invest. Ophthalmol. Vis. Sci.*, **39**, 2121–2131.
Seiler, M.J., Sagdullaev, B.T., Woch, G., Thomas, B.B. & Aramant, R.B. (2005) Transsynaptic virus tracing from host brain to subretinal transplants. *Eur. J. Neurosci.*, **21**, 161–172.
Seiler, M.J., Aramant, R.B. & Keirstead, H.S. (2008a) Retinal transplants: hope to preserve and restore vision. *Opt. Photonics News*, **19**, 37–47.
Seiler, M.J., Thomas, B.B., Chen, Z., Arai, S., Chadalavada, S., Mahoney, M.J., Sadda, S.R. & Aramant, R.B. (2008b) BDNF-treated retinal progenitor sheets transplanted to degenerate rats: improved restoration of visual function. *Exp. Eye Res.*, **86**, 92–104.
Seiler, M.J., Thomas, B.B., Chen, Z., R., W., Sadda, S.R. & Aramant, R.B. (2008c) Retinal transplants restore visual responses – trans-synaptic tracing from visually responsive sites labels transplant neurons. *Eur. J. Neurosci.*, **28**, 208–220.
Seiler, M.J., Aramant, R.B., Thomas, B.B., Peng, Q., Sadda, S.R. & Keirstead, H.S. (2010) Visual restoration and transplant connectivity in degenerate rats implanted with retinal progenitor sheets. *Eur. J. Neurosci.*, **31**, 508–520.
Steinberg, R.H., Flannery, J.G., Naash, M., Oh, P., Matthes, M.T., Yasumura, D., Lau-Villacorta, C., Chen, J. & LaVail, M.M. (1996) Transgenic rat models of inherited retinal degeneration caused by mutant opsin genes [ARVO abstract]. *Invest. Ophthalmol. Vis. Sci.*, **37**, S698.
Strettoi, E., Pignatelli, V., Rossi, C., Porciatti, V. & Falsini, B. (2003) Remodeling of second-order neurons in the retina of rd/rd mutant mice. *Vision. Res.*, **43**, 867–877.
Strettoi, E., Mears, A.J. & Swaroop, A. (2004) Recruitment of the rod pathway by cones in the absence of rods. *J. Neurosci.*, **24**, 7576–7582.
Suzuki, T., Akimoto, M., Imai, H., Ueda, Y., Mandai, M., Yoshimura, N., Swaroop, A. & Takahashi, M. (2007) Chondroitinase ABC treatment enhances synaptogenesis between transplant and host neurons in model of retinal degeneration. *Cell Transplant.*, **16**, 493–503.
Thomas, B.B., Seiler, M.J., Sadda, S.R. & Aramant, R.B. (2004) Superior colliculus responses to light – preserved by transplantation in a slow degeneration rat model. *Exp. Eye Res.*, **79**, 29–39.
Thomas, B.B., Aramant, R.B., Sadda, S.R. & Seiler, M.J. (2005) Light response differences in the superior colliculus of albino and pigmented rats. *Neurosci. Lett.*, **385**, 143–147.
Turner, D.L. & Cepko, C.L. (1987) A common progenitor for neurons and glia persists in rat retina late in development. *Nature*, **328**, 131–136.
Uesugi, R., Yamada, M., Mizuguchi, M., Baimbridge, K.G. & Kim, S.U. (1992) Calbindin D-28k and parvalbumin immunohistochemistry in developing rat retina. *Exp. Eye Res.*, **54**, 491–499.
West, E.L., Pearson, R.A., Tschernutter, M., Sowden, J.C., Maclaren, R.E. & Ali, R.R. (2008) Pharmacological disruption of the outer limiting membrane leads to increased retinal integration of transplanted photoreceptor precursors. *Exp. Eye Res.*, **86**, 601–611.
Woch, G., Aramant, R.B., Seiler, M.J., Sagdullaev, B.T. & McCall, M.A. (2001) Retinal transplants restore visually evoked responses in rats with photoreceptor degeneration. *Invest. Ophthalmol. Vis. Sci.*, **42**, 1669–1676.
Yang, P.B., Seiler, M.J., Aramant, R.B., Yan, F., Mahoney, M.J., Kitzes, L.M. & Keirstead, H.S. (2010) Trophic factors GDNF and BDNF improve function of retinal sheet transplants. *Exp. Eye Res.*, **91**, 727–738.
Zhang, Y., Arner, K., Ehinger, B. & Perez, M.T. (2003) Limitation of anatomical integration between subretinal transplants and the host retina. *Invest. Ophthalmol. Vis. Sci.*, **44**, 324–331.